Supporting Information

Si, B-containing dynamic covalent bonds enable excellent flame retardancy and reduced fire hazards for cyanate ester resin

Rui Liu, Yifeng Zhang, Zheng Li, Rui Wang, Hongxia Yan*

Supporting information S1

S1.1. Materials

4, 4'-Dihydroxybenzophenone (DHB) was provided by Shanghai Aladdin Biochemical Technology (Shanghai, China) Co., Ltd. 3-(Glycidoxypropyl) triethoxysilane (A187) was purchased from Jingzhou Jianghan Fine Chemical (Jingzhou, China) Co., Ltd. Tributyl borate (TBB) was obtained from Shanghai Macklin Biochemical (Shanghai, China) Co., Ltd. Bisphenol A cyanate ester (BADCy) resins were received from Jiangsu Wuqiao Resin Factory (Jiangsu, China) Co., Ltd. The used solvents such as N, N-dimethylformamide (DMF) and tetrahydrofuran (THF) were provided from Guangdong Guanghua Sci-Tech (Guangdong, China) Co., Ltd. No further purification was performed for all the raw materials. Common experimental apparatus such as flask and stirrer were supplied from Xi'an Haotian Chemical Glass Instrument (Shanxi, China) Co., Ltd.

S1.2. Characterizations

^{1}H nuclear magnetic resonance (^{1}H NMR) was detected on Bruker Avance 400 MHz spectrometer by using DMSO as solvent. Fourier transform infrared spectra (FTIR) was tested in the region of 400 to 4000 cm^{-1} on Nicolet FTIR 5700 spectrometer (U.S.A) with a resolution of 0.5 cm^{-1}. The gel permeation chromatography (GPC) of

Agilent 1260 (U.S.A) with tetrahydrofuran (THF) as mobile phase was adopted to test the molecular weight of synthetic polymers. The curing property was investigated by differential scanning calorimetry (DSC, Mettler-Toledo, Switzerland) with both isothermal (10 $K \cdot min^{-1}$) and non-isothermal methods (5 $K \cdot min^{-1}$ ~ 15 $K \cdot min^{-1}$) from 50 °C to 350 °C under N_2 atmosphere.

According to GB/T 2567-2008 (Chinese standard), the flexural strength was measured by electro-mechanical universal testing machine (CMT 6303) with the sample dimension of 80 mm × 15 mm × 4 mm^3. The impact strength was tested on the impact testing machine with the sample dimension of 80 mm × 10 mm × 4 mm^3. Five specimens were provided for each sample to decrease the error. The morphology of impact fracture surface was further detected on Scanning Electron Microscope (SEM, FEI Verios G4, U.S.A). Meanwhile, the microstructure of fabricated thermosets was observed on transmission electron microscope (TEM, FEI Talos F200X, U.S.A). The sample should be cut to obtain slices at room temperature by LEICA UC7 freezing microtome and stained by osmium tetroxide (OsO_4) for 20 minutes. Dielectric constant and loss of the samples were measured by coaxial-line method with Agilent PNA N5224A vector network analyzer in the X-band frequency range (8.2~12.4 GHz). The sample dimension was (22.86 ± 0.02) × (10.16 ± 0.02) × (2 ± 0.02) mm^3.

Thermogravimetric (TG) analyses were conducted on simultaneous thermal analysis (STA 449F3, Germany) with heating rate of 15 $°C \cdot min^{-1}$ under nitrogen atmosphere. Dynamic Mechanical Analysis (DMA) scans were performed using DMA/SDTA861e apparatus from 50 °C to 350 °C with a heating rate of 10 $°C \cdot min^{-1}$ at

1 Hz. The sample dimension was (65 ± 0.02) × (6 ± 0.02) × (3 ± 0.02) mm^3. The limited oxygen index (LOI) test was tested according to GB/T 2406.2-2009 (Chinese standard) by ZR-01 oxygen index meter (Qingdao, China) with the sample size of 80 mm × 10 mm × 4 mm^3. The UL 94 vertical burning test was conducted on a ZR-02 instrument according to ASTM D3801 standard with the specimen dimension of 125 × 13 × 4 mm^3. Cone calorimeter test was measured on FTT Cone Calorimeter at a heat flux of 35 kW/m^2 with the dimension size was 100 × 100 × 4 mm^3 according to ISO 5660 standard. The surface elements of combustion samples were investigated by X-ray Photoelectron Spectroscopy (XPS) under power of 150 W with the aluminum target (Al Kα hυ=1486.6 ev) as X-ray source. Raman spectrum was employed on Alpha300R Raman spectroscopy equipped with 532 nm TEM00 laser. Thermogravimetric analysis/infrared spectrometry (TG-IR) in the air atmosphere was conducted on thermal analysis (STA449 F5 Jupiter, Germany) equipped with an infrared spectrometer (Nicolet iS50, U.S.A) with a heating rate of 10 $K \cdot min^{-1}$.

Supporting information S2

S2.1. Synthesis of HPSiB

HPSiB was synthesized via one-pot transesterification polycondensation. Specifically, 6.4266 g DHB was dissolved in 20 mL DMF at first and transferred the solution to a 150 mL three-necked flask equipped with a mechanical stirrer. Then 5.5684 g A187 was added into the flask to perform the reaction from 90 °C to 140 °C until no distillate generation, with stirring under N_2 atmosphere. Whereafter, the

temperature was reduced to 90 °C and 4.6030 g TBB was added to continue the reaction with the temperature range from 90 °C to 160 °C. After 24 h reaction, the crude product was purified by reduced pressure distillation to remove the solvent. Further purification of dialysis was conducted to reap expected HPSiB with high molecular weight, using the dialysis tube of molecular weight cut off is 5000.

S2.2. Fabrication of HPSiB/BADCy resin

The HPSiB/BADCy resins were prepared via the copolymerization of BADCy and HPSiB. Firstly, 80 g BADCy was melted at 100 °C to perform the crosslinking reaction with different amount of HPSiB in a 250 mL beaker under mechanical stirring at 130 °C for 1 hour. Then the HPSiB/BADCy prepolymer was deaerated for 1.5 hours and transferred into a preheated mold to cure following the procedure of 160 °C/2 h+180 °C/2 h+200 °C/2 h+220 °C/2 h. Finally, the HPSiB/BADCy thermosets were gained after demolded at cooling to room temperature. The HPSiB/BADCy systems with various HPSiB addition (2 wt%, 4 wt%, 6 wt%, 8wt%) were marked as BADCy-x, where x represents HPSiB addition.

Supporting information S3

S3.1. Structural characterizations of HPSiB

There are two steps with different distillate in the synthesis process of HPSiB due to its A3+B2+C3 polycondensation reaction. The two reaction distillates of ethanol and 1-butanol have confirmed the execution of polycondensation in Fig. S1b. Further characterization was conducted for the A187, DHB, TBB and synthesized HPSiB. As

shown in Fig. 1b, the peak at 3341 cm^{-1} is correlated to stretching vibration of -OH in DHB spectra, while the peak widens in P1 spectra due to the association of hydroxyl groups. Meanwhile, the characteristic peaks of Si-O-C at 1075 cm^{-1} and epoxy groups at 912 cm^{-1} were detected in HPSiB spectra.[1] Notably, the signals of B-O bonds at 1327 & 1421 cm^{-1} in TBB spectra, which shift to 1390 & 1434 cm^{-1} in P2 spectra due to the conjugate average effect of hyperbranched polymer.[2]

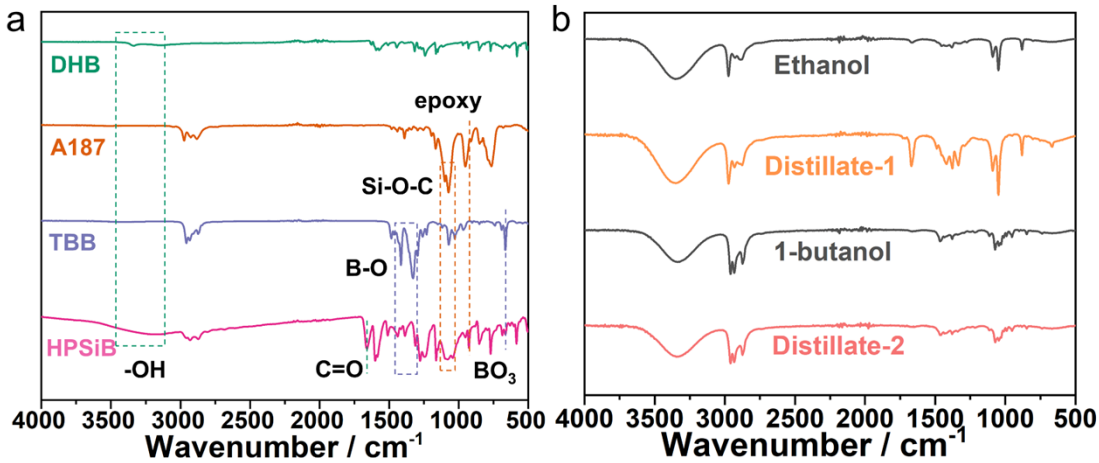

Fig. S1 FTIR spectra of (a) DHB, A187, TBB and HPSiB; (b) two reaction distillates and standard ethanol and 1-butanol.

^{1}H-NMR spectra were further adopted to demonstrate the structure of HPSiB. As exhibited in Fig. S2, the proton signals of alkoxy groups for the two monomers were still identified, indicating the incomplete reaction due to the large steric hindrance. The proton signals belonged to the polymer skeleton also present at the spectra, including the protons of benzene rings and epoxy groups. Nevertheless, a significant change occurs in the signal of hydroxyl, which emerges at 7.05 ppm, suggesting the effect of proceeded reaction on the proton signal. The ^{1}H-NMR and FT-IR spectra initially support the proposed structure of HPSiB.

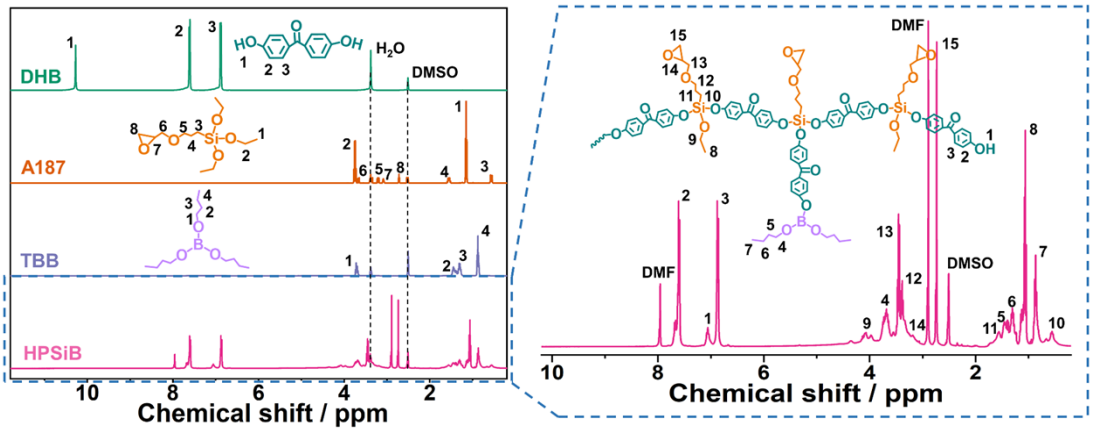

Fig. S2 ^{1}H-NMR spectra of DHB, A187, TBB and HPSiB.

In addition, the GPC curve of HPSiB exhibited a broad molecular weight distribution in the retention time located on 23.0~24.1 min with PDI of 1.023, implying the homogeneous molecular weight achieved by long-time polymerization (Fig. S3). It has a high molecular weight, evidenced by a number average molecular weight *Mn* of 26098 g/mol and a weight average molecular weight *Mw* of 26697 g/mol.

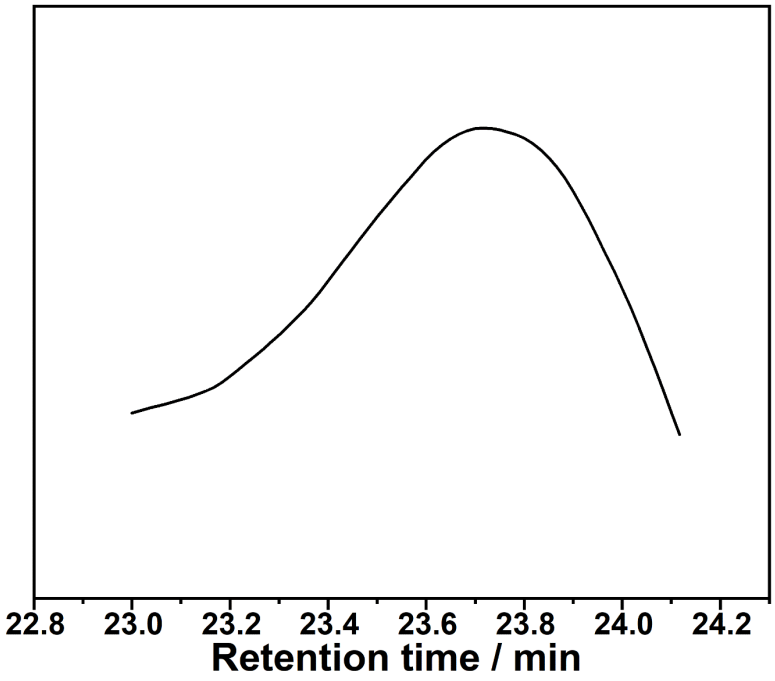

Fig. S3 GPC curve of HPSiB in THF

Table. S1 Molecular weight and distribution of HPSiB

Polymer	$\bar{M}p$	$\bar{M}n$	$\bar{M}w$	$\bar{M}z$	PDI($\bar{M}w/\bar{M}n$)
HPSiB	25578	26098	26697	27337	1.023

Moreover, the degree of branching (DB) of HPSiB was calculated by Fréchet Eqn (1):[3]

$$DB = \frac{D+T}{D+T+L} \tag{1}$$

The D, T, L are dendritic units, terminal units, the linear units, respectively. As shown in Fig. S4, ^{1}H-NMR integral gives the corresponding D, L and T units, where H8H9 are assigned to L units. The H2H3 are corelated to D, L and T units. The detail calculation of DB is as follow:

$$L = \frac{1.11}{3} + \frac{0.51}{2} = 0.625 \tag{2}$$

$$D+T+L = \frac{1.00+0.79}{1} = 1.79 \tag{3}$$

$$DB = \frac{D+T}{D+T+L} = 0.65 \tag{4}$$

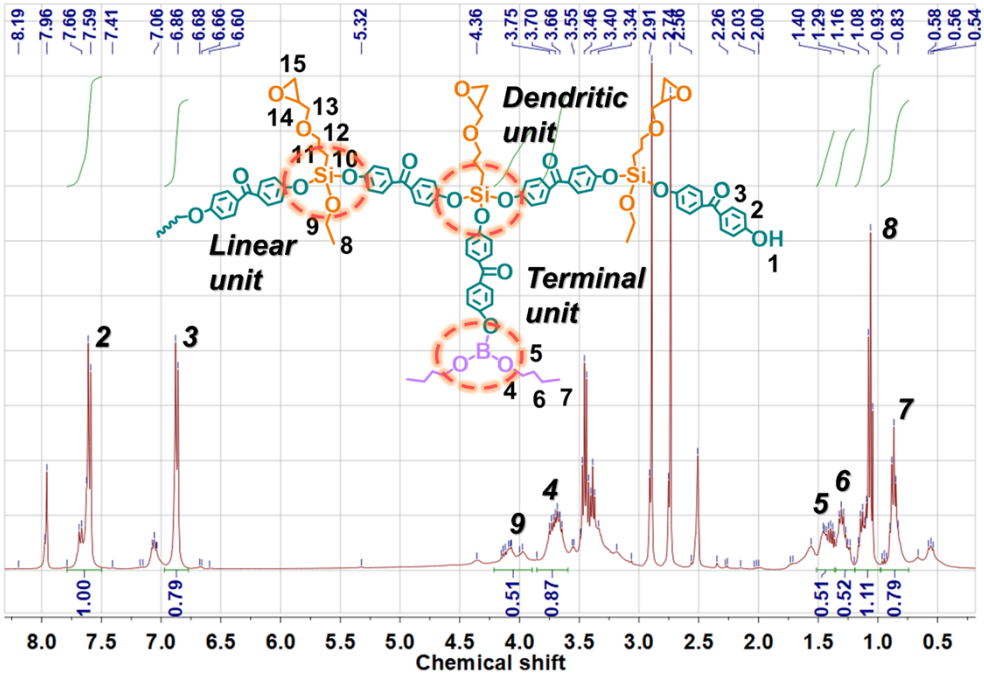

Fig. S4 ^{1}H-NMR of HPSiB and the peak integral

Supporting information S4

S4.1. Curing behavior of BADCy and BADCy-6 prepolymer

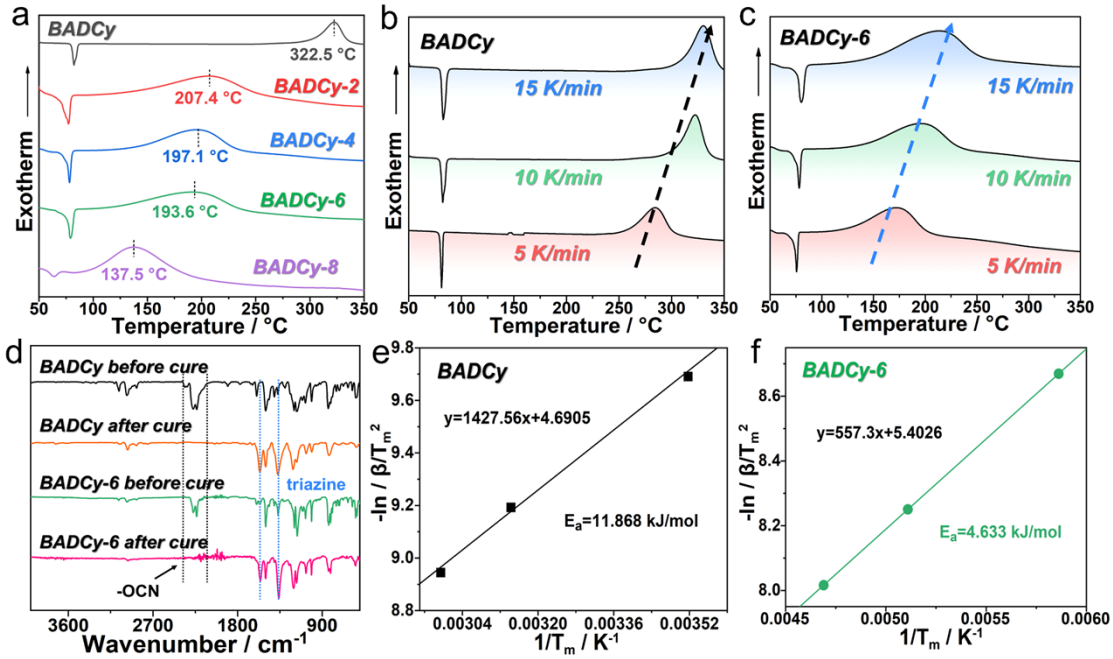

Fig. S5 DSC curves of (a) BADCy and BADCy-X prepolymer at the heating rate of 10 K/min, BADCy (b) and BADCy-6 (c) prepolymer at different heating rates; FT-IR spectra of BADCy and BADCy-6 before/after cure (d); Linear relation of $-\ln(\beta/T_m^2)$ and $1/T_m$ of BADCy (e) and BADCy-6 (f).

Curing behavior is the critical factor in determining material properties, in addition to affecting the preparation process. The effect of HPSiB addition on the curing behavior of the BADCy system was firstly investigated at the heating rate of 10 K/min. As shown in Fig. S5, a single endothermic peak and exothermic peak were detected in all BADCy systems, corresponding respectively to the melting and curing of the resin system. The endothermic peak temperature changed slightly, whereas the exothermic peak temperature decreased sharply with the HPSiB addition. In particular, BADCy-8 exhibited a significant 185 °C reduction in the exothermic peak temperature. This

manifests the rapid catalysis of HPSiB on the curing reaction of BADCy resin. Nevertheless, redundant HPSiB may generate the local excessive crosslinking contributed to stress concentration for deteriorated mechanical performance.[4] Therefore, BADCy-6 was chosen for the study of the HPSiB effect on the curing reaction of BADCy system.

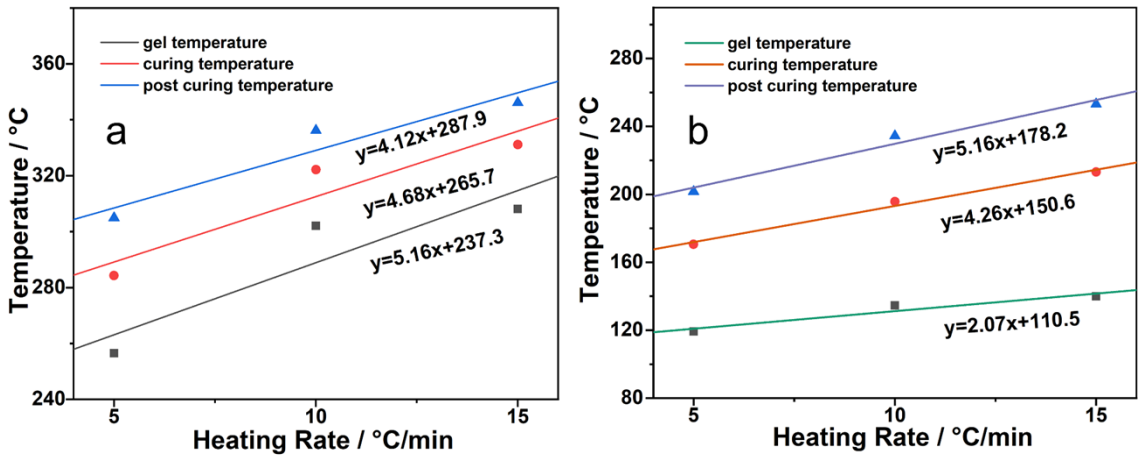

Fig. S6 DSC linear fitting diagram of BADCy (a) and BADCy-6 prepolymer (b).

DSC curves of BADCy and BADCy-6 system at different heating rates were tested to get the initial temperature, peak temperature and final temperature (Fig. S5b-c). They were further employed to linear fitting to obtain gel point, cure temperature and post cure temperature as a reference for curing process (Fig. S6). Meanwhile, the apparent activation energy of BADCy (11.868 kJ/mol) and BADCy-6 (4.633 kJ/mol) was calculated via Kissinger equation detailed in Supporting information S4.2. The significant reduction in apparent activation energy of BADCy-6 exactly demonstrates the effective catalysis of HPSiB in the curing reaction.[5]

Further, FT-IR spectra was employed to analyze the curing reaction mechanism. Fig. S5d presents that the characteristic peak of cyano groups vanished and the

absorption peaks of triazine emerged after curing in both BADCy and BADCy-6 spectra. This suggests that the curing process mainly involves the trimerization of cyano groups. Regarding to the significant reduction in curing temperature of BADCy-6 system, it is subject to the catalysis of active hydrogen in the terminated hydroxyl groups of HPSiB.[6] The detailed reaction mechanism of BADCy-6 system provided in Fig. S7.

Table S2 Exothermic temperature of BADCy prepolymer

Heating rate/K/min	5	10	15
Initial temperature	256.5	302.1	308.1
Peak temperature	284.3	322.2	331.1
Final temperature	304.9	336.2	346.1

Table S3 Exothermic temperature of BADCy-6 prepolymer

Heating rate/K/min	5	10	15
Initial temperature	119.2	134.6	139.9
Peak temperature	134.2	195.7	213.2
Final temperature	139.9	234.5	253.2

Table S4 Curing temperature of BADCy and BADCy-6 prepolymer

Polymer	Gel point	Curing temperature	Post curing temperature
BADCy	237.3	265.7	287.9
BADCy-6	110.5	150.6	178.2

S4.2 Apparent activation energy of BADCy and BADCy-6 thermosets

As shown in Kissinger equation (1), ΔE, β and R is respectively apparent activation energy, heating rate and ideal gas constant. The ideal gas constant is a constant of 8.314. Hence, the apparent activation energy can be calculated once the slope of linear relation of $-\ln(\beta/T_m^2)$ and $1/T_m$.

$$\frac{d\left[ln\left(\beta/{T_m}^2\right)\right]}{d\left[1/T_m\right]} = -\Delta E/R \quad (1)$$

Fig. S5e-f displays the linear relation of $-\ln(\beta/T_m^2)$ and $1/T_m$ in BADCy and BADCy-6. The slope of linear relation for BADCy and BADCy-6 is -1427.56 and -557.3, severally. Therefore, the apparent activation energy of BADCy and BADCy-6 is respectively 11.868 kJ/mol and 4.633 kJ/mol. The significantly reduced apparent activation energy of BADCy-6 indicates its high curing reaction speed.

Supporting information S5

Table S5 UL-94 and LOI results of BADCy and BADCy-X systems.

Samples	UL-94			LOI (%)
	Rating	t1+t2 (s)	Dripping	
BADCy	No rating	(61.2+3.6) ± 0.32	No	26.6 ± 0.31
BADCy-2	V-1	(21.9+1.3) ± 0.43	No	27.8 ± 0.16
BADCy-4	V-1	(15.4+0.7) ± 0.11	No	29.4 ± 0.30
BADCy-6	V-0	(8.0+0.0) ± 0.11	No	32.8 ± 0.27
BADCy-8	V-1	(26.7+0.5) ± 0.25	No	28.8 ± 0.31

Table S6 Data of BADCy and BADCy-6 in cone calorimeter test.

Samples	TTI (s)	TTF (s)	TTpHRR (s)	pHRR ($kW \cdot m^{-2}$)	COY/ CO_2Y(%)	TOC (g)	Residue (wt%)	FGR ($kW \cdot m^{-2} \cdot s^{-1}$)	FPI ($m^2 \cdot s \cdot kW^{-1}$)
BADCy	158	2131	10	263.3	17.5	163.8	12.0	26.3	0.6
BADCy-6	162	1755	20	246.1	16.0	68.6	20.7	12.3	0.7

Table S7 Energy gap of single molecules for BADCy and BADCy-6.

Polymer	E(HOMO) (eV)	E(LUMO) (eV)	Energy gap (eV)	Energy gap (a.u.)
BADCy	-6.416281	-1.104715	5.311566	0.195196
BADCy-6	-6.108869	-2.256531	3.852337	0.141571

Table S8 UL-94 raw data of BADCy and BADCy-X systems.

Sample	Time (s)	S1	S2	S3	S4	S5	AVERAGE	STDEV
BADCy	t1	61.3	61.2	61.1	61.4	61.2	61.24	0.114
	t2	3.8	3.9	3.5	3.4	3.6	3.64	0.207
BADCy-2	t1	21.5	21.8	21.9	22.2	22.3	21.85	0.321
	t2	1.1	1.3	1.3	1.2	1.4	1.26	0.114
BADCy-4	t1	15.3	15.4	15.5	15.3	15.4	15.38	0.084
	t2	0.68	0.65	0.72	0.71	0.69	0.69	0.027
BADCy-6	t1	7.96	7.89	8.05	8.15	8.08	8.026	0.102
	t2	0.01	0.03	0.01	0.00	0.01	0.012	0.011
BADCy-8	t1	26.4	26.5	26.8	26.9	26.7	26.66	0.207
	t2	0.48	0.45	0.51	0.53	0.55	0.504	0.0397

Table S9 LOI raw data of BADCy and BADCy-X systems.

Sample	S1	S2	S3	S4	S5	AVERAGE	STDEV
BADCy	26.9	26.5	26.1	26.8	26.5	26.56	0.313
BADCy-2	27.6	27.9	28.0	27.6	27.8	27.78	0.16
BADCy-4	29.8	29.2	29.5	29.3	29.0	29.36	0.304
BADCy-6	33.2	32.5	32.7	32.8	32.6	32.76	0.270
BADCy-8	28.6	28.7	29.3	28.8	28.5	28.78	0.311

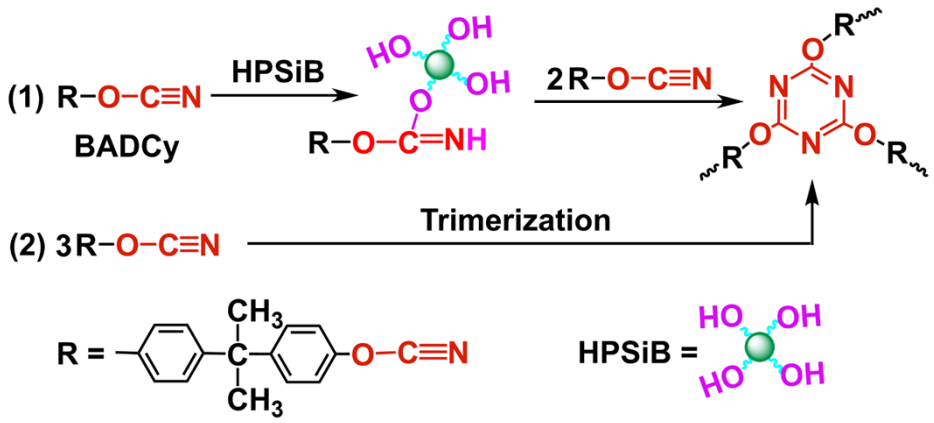

Fig. S7 The curing mechanism of HPSiB/BADCy system.

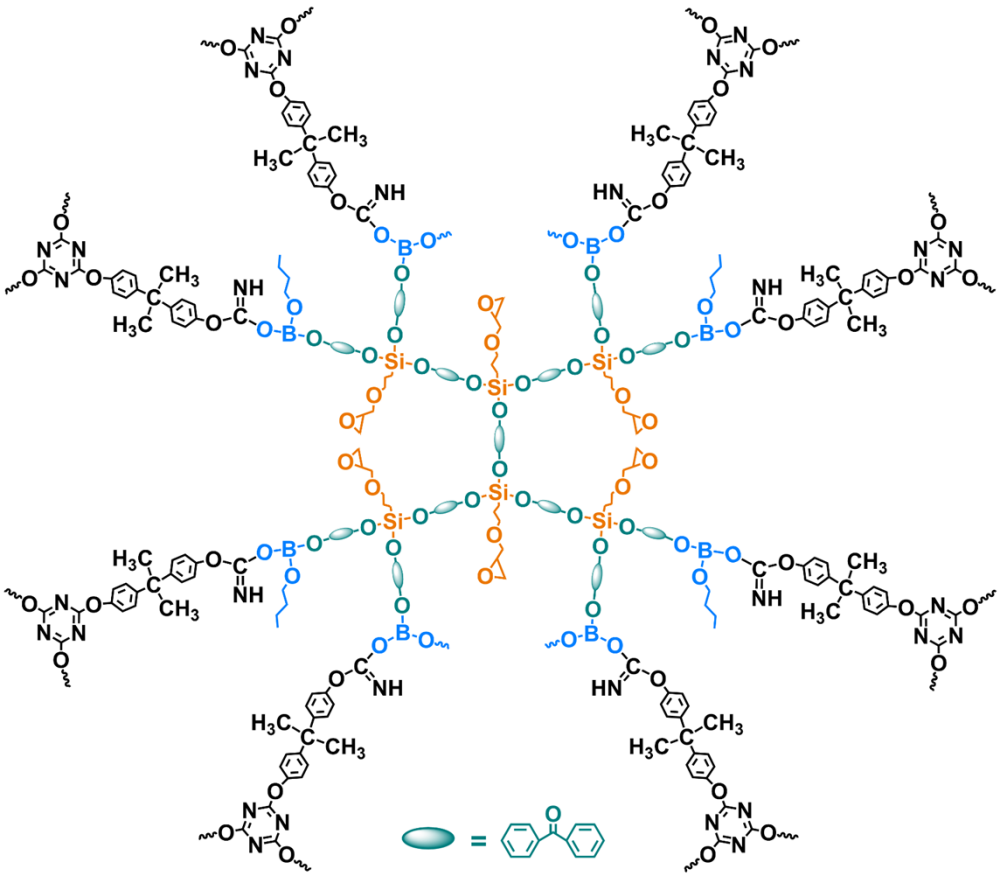

Fig. S8 The chemical structure of HPSiB/BADCy.

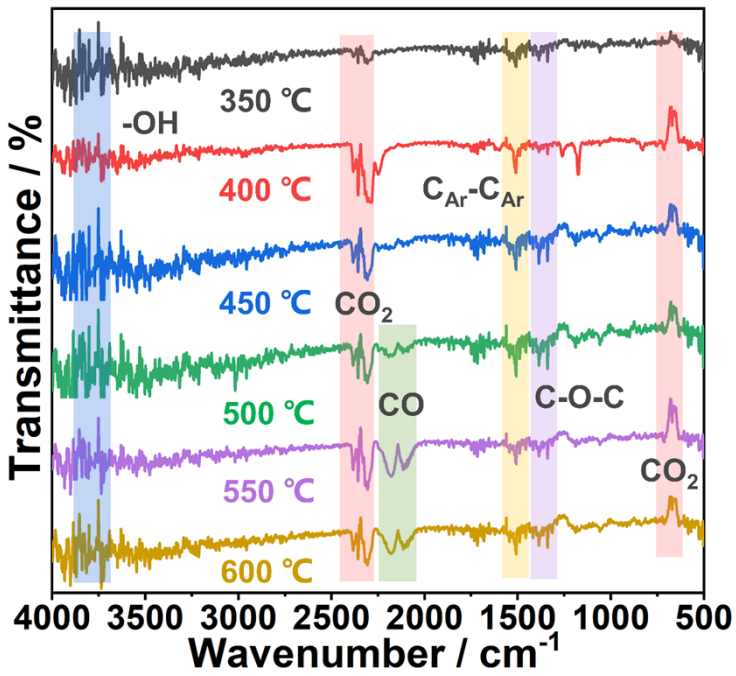

Fig. S9 TG-IR spectra of BADCy.

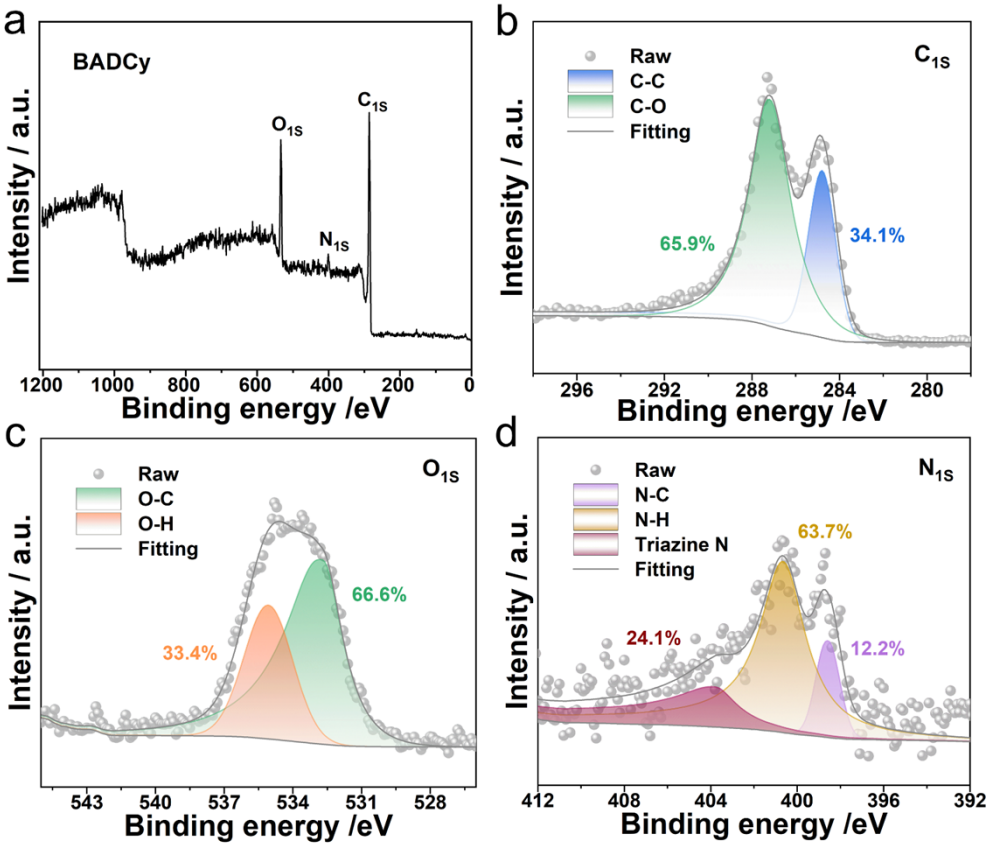

Fig. S10 XPS curves of the full-scan spectrum (a), C1s (b), O1s (c), and N1s (d) for the char residues of BADCy.

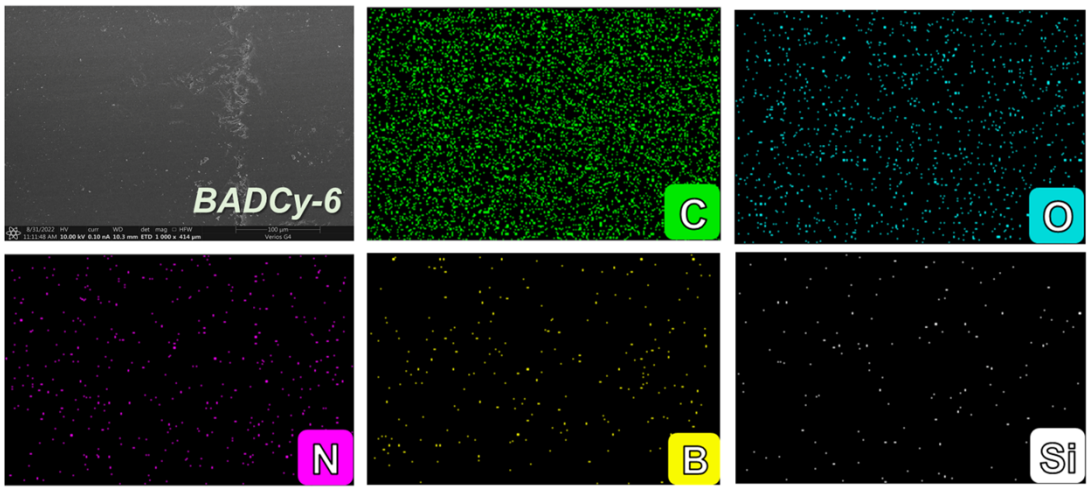

Fig. S11 The element mapping for BADCy-6 char residues.

Supporting information S6

S6.1. The calculation of network crosslinking density

According to rubber elasticity theory, the crosslinking density ($d_{crosslink}$) of a polymer network can be determined via the dynamic thermomechanometry method,[4] utilizing Equation (1). The resultant calculations are tabulated in Table S10.

$$d_{crosslink} = E'/[2(1+\gamma)RT] \quad (1)$$

In this formulation, E' denotes the rubbery plateau storage modulus evaluated at (T_g + 40) °C; γ represents Poisson's ratio, typically assumed to be 0.5 for an incompressible crosslinked network within thermoset materials; R signifies the gas constant, while T is the temperature of (T_g + 40) °C. It is crucial to note that this equation is specifically applicable to lightly crosslinked materials, serving solely as a qualitative tool for assessing crosslinking levels in casting resins.

Table S10 DMA parameters for calculating the crosslinking density of BADCy-X.

Sample	T_g/°C	E' at (T_g + 40°C)/MPa	$d_{crosslink}$/mol·m^{-3}
BADCy	232.2	12.0654	1.78×10^{-3}
BADCy-2	256.4	13.5769	1.84×10^{-3}
BADCy-6	267.2	15.6691	2.04×10^{-3}
BADCy-8	215.1	17.3249	2.72×10^{-3}

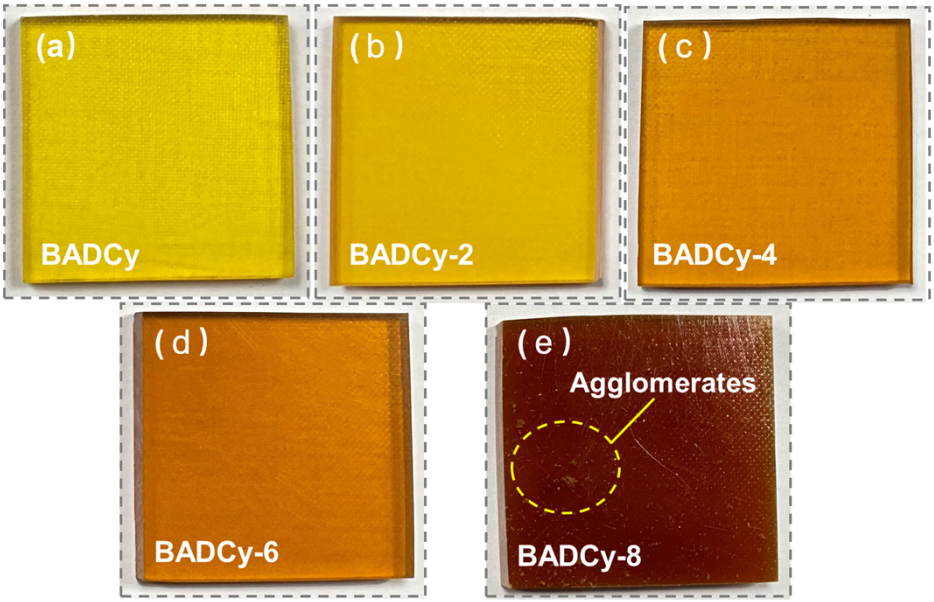

Fig. S13 Digital photos of BADCy and BADCy-X samples.

References

[1] S. Niu, H. Yan, S. Li, C. Tang, Z. Chen, X. Zhi and P. Xu, *J. Mater. Chem. C*, 2016, **4**(28), 6881.

[2] L. Guo, L. Yan, Y. He, W. Feng, Y. Zhao, B.Z. Tang and H. Yan, *Angew. Chem. Int. Edit.*, 2022, **61**(29), e202204383.

[3] Y. Zhang, H. Yan, G. Feng, R. Liu, K. Yang, W. Feng, S. Zhang and C. He, *Compos. Part B: Eng.*, 2021, **222**, 109043.

[4] R. Liu, H. Yan, Y. Zhang, K. Yang and S. Du, *Chem. Eng. J.*, 2022, **433**, 133827.

[5] J. Li, Q. Cao, Y. Zhao, C. Gu, B. Liu, Q. Fan, C. Zhang, Y. Huang, S. Jiang, X. Jian and Z. Weng, *Compos. Part B: Eng.*, 2024, **276**, 111362.

[6] X. Gu, Z. Zhang, L. Yuan, G. Liang and A. Gu, *Chem. Eng. J.*, 2016, **298**, 214.